How to Cite: Verekar, R.R., Shaikh, Sh.B.M., Rebelo, S., & Gurav, Sh.S. (2025). Double-Loaded Liposomes Encasing Umbelliferone in Hydroxypropyl-β-Cyclodextrin Inclusion Complexes: Formulation, Characterisation and Investigation of Photoprotective Activity. *Eurasian Journal of Chemistry, 30, 2(118), 34-51.* https://doi.org/10.31489/2959-0663/2-25-15

Article

Received: 20 March 2025 | Revised: 21 May 2025 |
Accepted: 27 May 2025 | Published online: 24 June 2025

UDC 547-3; 542.8

https://doi.org/10.31489/2959-0663/2-25-15

Rucheera R. Verekar[1], Shamshad Bi M. Shaikh[2], Sarita Rebelo[2], Shailendra S. Gurav[1*]

[1]*Department of Pharmacognosy, Goa College of Pharmacy, Goa University, Goa, India;*
[2]*School of Biological Sciences and Biotechnology, Goa University, Taleigao Plateau, Taleigao, Goa, India*
*(*Corresponding author's email: shailendra.gurav@nic.in)*

Double-Loaded Liposomes Encasing Umbelliferone in Hydroxypropyl-β-Cyclodextrin Inclusion Complexes: Formulation, Characterisation and Investigation of Photoprotective Activity

Double-loaded liposomes are a system in which a drug is incorporated in the vesicle lipid layers after aqueous phase inclusion complexation to form a drug-in-cyclodextrin-in phospholipid vesicles complex. Umbelliferone (UMB) is a naturally occurring coumarin used as a photoactive agent because of its UV light absorption ability. In this study, the double loading (DL) technique was used to encapsulate "UMB in hydroxy propyl-β-cyclodextrin (HP-β-CD)-in-liposomes (UMB-CDLP)". This led to the creation of "double-loaded liposomes encasing UMB in HP-β-CD (DL-UMB-CDLP)", specifically developed to combine the power of solubilisation of HP-β-CD with the sustained release characteristics of phospholipid vesicles to improve solubility and dissolution profile. HP-β-CD and UMB inclusion complexes prepared by different methods were characterized by FTIR spectroscopy, DSC, saturation solubility, x-ray diffractometry, and scanning electron microscopy. DL-UMB-CDLP was developed using a thin film/lipid hydration method and a Box-Behnken design and was assessed by TEM, *in-vitro* diffusion studies and biological evaluation. The optimized DL-UMB-CDLP formulation demonstrated promising results, indicating the development of a stable composition. Animals treated with the DL-UMB-CDLP gel and exposed to the immediate irradiation protocol proved the UMB's ability to protect against UV-induced oxidative damage based on the amount of antioxidant enzymes estimated to be present in rat skin.

Keywords: Umbelliferone, double-loaded liposome, inclusion complex, photoprotective activity, photoactive agent, irradiation protocol, drug-in-cyclodextrin, drug-in-phospholipid

Introduction

Numerous studies have been established on different plant secondary metabolites for their medicinal properties and general health-promoting potential using phytochemical and phytopharmacological research. However, their limited solubility in lipophilic solvents and hydrolytic instability at various physiological pH levels restrict their topical and oral absorption through the lipoidal biological membrane, which can be overcome by their structural modifications, phospholipid complexation, as well as the use solubility and bioavailability modifiers [1].

Cyclodextrins (CDs) are cyclic oligosaccharides derived from starch and their abridged cone shape with hydrophobic cavity and exterior hydrophilic surface allows them to form inclusion complexes with lipophilic drugs, which is a crucial factor to enhance their solubility and stability. Moreover, modified CDs, such as 2-hydroxypropyl-α/β/γ CD, enhances drug-binding abilities and solubility [2].

Liposomes, phospholipid vesicles, serve as a drug delivery strategy to enhance loading capacity, stability, sustained-release pattern and encapsulation of hydrophilic and lipophilic molecules resulting in better bioavailability [3]. There are situations where the molecule or molecules to be trapped are incompatible with the vesicles formation, and the addition of lipophilic molecules to vesicle lipid bilayers can negatively affect the bilayer development and ultimately their stability. In therapy, increasing phospholipid levels to support higher drug concentrations may not be possible for obvious reasons [4, 5]. McCormack and Gregoriadis [6] developed a drug-in-cyclodextrin-in phospholipid vesicle system, also known as double-loading (DL) of the drug, by incorporating a drug into the vesicle lipid layers following aqueous phase inclusion complexation [6, 7]. Several reports employing DL of curcumin [2], lycopene [5], paclitaxel [8], quercetin [9], etc., in β-CD have confirmed their enhanced stability and bioavailability.

Acute and long-term inflammatory alterations such as erythema, immunosuppression, photoaging, and carcinogenesis are caused by exposure to ultraviolet (UV) radiation, which also damages the skin clinically and histologically [10–12]. Extrinsic ageing or photoaging (a term describing skin aging caused by cumulative solar UV radiation) is a complex biological process that affects the skin's structural integrity and physiological activity. Long-term exposure of the skin to solar UV radiation increases free radicals and reactive oxygen species (ROS), triggering signaling pathways and facilitating inflammatory reactions through inflammatory cytokines like tumor necrosis factor (TNF-α) and interleukins (IL) of types 1 (IL-1) and 6 (IL-6) [13–15]. Furthermore, oxidative stress is also caused by high levels of ROS. The redox equilibrium cannot be maintained in this situation due to the inadequacy of natural antioxidant defence systems such as the enzymes superoxide dismutase and catalase. Consequently, excess ROS are associated with the skin aging process and have harmful effects on the body [16–18].

The use of dermatological preparations with UV filters is considered the most effective cosmetic strategy to counteract the negative effects of UV radiation [19, 20]. However, they are useless in providing complete protection due to their failure to tackle the biochemical processes leading to UV-induced tissue damage [12]. Furthermore, concerns about the ecological and human safety of filters are pushing the scientific community to look for new options [21, 22]. Plant-derived anti-inflammatory and radical scavengers are proven as promising photoprotective agents against UVA-UVB radiation damage [23, 24].

Umbeliferone (UMB), 7-OH hydroxycoumarin, is a yellowish-white crystalline compound found abundantly in plants, belongs to the Apiaceae family and a few other species, such as *Hieracium pilosella* (Asteraceae) and *Hydrangea macrophylla* (Hydrangeaceae) [25]. A hydroxyl group of UMB interact with phosphatidylcholine's polar choline group to form a UMB-phospholipid complex. Since UMB offers the necessary qualities, the current study formulates it as a UMB-in-cyclodextrin-in phospholipid complex (UMB-CDLP) to enhance its solubility, permeability, antioxidant activity, and decisive photoprotective action. The main goal was to protect UMB from oxidation, heat and light. It has been suggested that this complex formation stabilizes the trapped molecule against various chemical attacks [6, 7]. The aim of this study was to create a UMB-in-CD-in-phospholipid vesicles that would combine the sustained-release pattern of phospholipid vesicles with the solubilizing ability of β-CD. Further, the study extends toward incorporating DL-UMB-CDLP into a semi-solid vehicle to design a final gel formulation for topical application.

Experimental

Materials

UMB was purchased fromTokyo Chemical Industry (TCI), and its purity was >98 %. A gratis sample of Phospholipon@90H (PL90H) was acquired from Lipoid Germany. The cholesterol used was of analytical grade and was supplied by Molychem, Mumbai. The ethanol used was of laboratory grade. The other reagents and chemicals were all analytical grade. The assay kits for antioxidant marker enzyme estimation were purchased from Elabscience USA.

Methodology

Preparation of UMB-β-CD Molecular Inclusion Complexes

Four different methods were used to prepare the UMB-β-CD molecular inclusion complex.

Physical Mixture Method

The necessary molar ratios (1:1, 1:2, and 1:3) of hydroxy propyl-β-cyclodextrin (HP-*β*-CD) and drug UMB were weighed and combined separately in a mortar by trituration for 5 min. After passing through a #40 sieve, the mixtures were kept in an airtight container until they were needed again [26].

Kneading Method

Precisely weighed molar amounts of each HP-β-CD were mixed with a moistening agent consisting of distilled water and ethanol (1:1). Molar amounts of the drug were added with continuous grinding. The consistency of the pastes was maintained during the 1 hour grinding process using the required amount of moistening agent. Finally, these pastes were dried for 24 hours at 55 °C in a hot air oven. After passing the dried pastes through sieve #40, the leftover mass was gathered and kept in airtight containers until needed again [27, 28].

Solvent Evaporation Method

Distilled water was used in this method to dissolve the drug and HP-β-CD. The resultant mixture was vacuum evaporated at 55 °C stirring for 24 hours to obtain a pure solution. After being dried, the material was pulverised to a powder and run through a sieve #40 [26].

Co-Evaporation Method

To obtain a solid powdered inclusion complex, this technique involves separately dissolving the drug and HP-β-CD in two mutually miscible solvents, such as ethanol and water, respectively, mixing the two solutions to create a molecular dispersion of the drug and complexing agents, and then vacuum evaporating the solvent. After stirring the mixture for an entire day, it was vacuum evaporated at 55 °C. After being pulverised, the dried mass was run through a sieve #40 [2, 27, 28].

Optimization of UMB-β-CD Molecular Inclusion Complex

The percent yield was determined to find the best inclusion complex method and was estimated using the following formula:

$$\text{Percent yield} = \frac{\text{Practical mass}}{\text{Theoretical Mass}\left(\text{Drug}+\text{Carrier}\right)} \times 100\,\% .$$

Drug content was estimated with the help of the reported methods using UV spectrophotometer at 345.5 nm. The detailed procedures are presented in the Supplementary Materials file [29].

Dissolution Studies

Each inclusion complex sample equivalent to 10 mg of UMB was subjected to a dissolution test using Dissolution Test Apparatus USP (Type–II). A comparable dissolution test was performed using 10 mg of pure UMB as a control. The dissolution medium had a volume of 500 mL and consisted of PBS 7.4. The apparatus was operated after adding an inclusion complex equivalent to 10 mg of UMB to the dissolution medium (PBS 7.4). The temperature was held at 37 ± 0.5 °C while the stirring speed was set at 50 rpm. 5 mL aliquots from the dissolution medium were removed using a 0.45 µm membrane filter (Ustar LB, USA) at 1, 3, 5, 7, 10, 12, 15, 20, 25, 30, 45, and 60 min. An equal volume of the freshly prepared dissolution medium was then added. Spectrophotometric measurements using a UV-visible spectrophotometer (Shimadzu, UV-2700) of UMB concentrations at 324.5 nm were performed using the standard curve's regression equation generated in the same medium. Three duplicates of each experiment were performed and the mean value was determined [28].

Characterisation of Optimized UMB-β-CD Molecular Inclusion Complex

The physicochemical characterisation [5, 28, 30–33] of the plain drug, PL90H, cholesterol, HP-β-CD, physical mixture (PM) and inclusion complex was carried out using various techniques such as FT-IR analyses (FTIR spectrophotometer IR Affinity-1S, Shimadzu), saturation solubility analysis, Differential Scanning Calorimetry (DSC) analysis (TA Instruments, Q20, USA), X-ray diffraction (XRD) analysis (D2 Phaser, Bruker AXS, USA), Scanning electron microscopy (SEM) (JEOL Mode Japan JSM 639OLV) at University Science Instrumentation Center (USIC), Goa University, Goa. The detailed procedures for all the analyses are given in the Supplementary Materials file.

Formulation Development of DL-UMB-CDLP- QbD Approach

DL-UMB-CDLP was prepared using film/lipid hydration methodology and the quality-by-design (QbD) approach. The required lipids (PL90H : cholesterol) were taken in different molar ratios (5:5, 7:3, 9:1) along with **C5** complex (Table S3) equivalent to 100 mg of UMB and dissolved in ethanol. The obtained organic solvent was slowly removed using a rotary evaporator at 37 °C ± 2 °C. The lipid film deposited on the flask's inner walls was hydrated by adding 10 mL of PBS (pH 7.4). The obtained liposome suspension was subjected to stirring on a magnetic stirrer for 3 hours at the required RPM (600, 800, 1000 rpm) and then probe was sonicated for 10s on and 5s off pulse for 5 min at 40 % amplitude. Subsequently, centrifugation (15000 rpm, 4 °C, and 30 min) was performed to separate the pellet from the suspension. The liposomal suspension was stored in glass vials [5].

Table 1

Coded level and Real values for each factor under study for DL-UMB-CDLP formulations

Variables	Level		
	–1	0	+1
Independent	Real Values		
PL90H : Cholesterol (X1)	5:5	7:3	9:1
Lipid : Drug (X2)	1:1	2:1	3:1
Stirring Speed (X3)	600	800	1000
Dependent: Entrapment Efficiency and Particle Size			

StatEase Inc's Design Expert software (version 10) was used for the design experiments. Three factors and three levels of Box-Behnken design were used to carry out the optimization. This study employed a 3^3 randomised full factorial design employing PL90H : Cholesterol ratio (X1), Lipid : Drug ratio (X2), and stirring speed (X3) to determine the effect of those three independent factors on entrapment efficiency and particle size (Table 1). Three levels, numbered +1, 0, and –1, were used to test each component. F-statistics were utilised to assess the response [34]. Variables in the model were deemed significant if their *p*-values were higher than 0.05. The association between the responses and independent variables was ascertained utilising two-dimensional contour plots [5].

Evaluation of the DL-UMB-CDLP

Entrapment Analysis

An indirect method of entrapment analysis was carried out to calculate the entrapment efficiency of a drug. The entrapment efficiency was determined after centrifugation of DL-UMB-CDLP suspension at 15000 rpm, at 4 °C for 30 min. A solvent in which the drug is highly soluble, but the complex is not, was used to separate the unentrapped drug fraction. The free drug was estimated by UV analysis. Based on the absorbance range, the formulation batches were dispersed in 10 mL of ethanol; further dilutions were made in PBS 7.4. The UV absorbance was determined at 324.5 nm for DL-UMB-CDLP [25, 35]. The formula given below was used to assess entrapment efficiency:

$$\text{Entrapment Efficiency} = \frac{\text{Total Drug} - \text{Free Drug}}{\text{Total Drug}} \times 100\,\%\,.$$

Particle Size and Zeta Potential Analysis

The prepared liposomal complex's particle size was determined using photon correlation spectroscopy with dynamic light scattering on a Zetasizer® nano (Malvern, ZSU3100) fitted with a 5 mW Helium-Neon laser with an output wavelength of 633 nm. Measurements were made with a runtime of at least 40 to 80 s, at a 90° angle, and at 25 °C. Smoluchowski's equation was used to determine the zeta potential based on the electrophoretic mobility of liposomes [36].

Differential Scanning Calorimetry (DSC) Analysis

One of the most well-known calorimetric techniques for studying solid-phase interactions of drugs with polymers is DSC. The optimized formulation and pure drug samples were heated in aluminum pans with flat bottoms between 70 °C and 320 °C at a constant rate of 10 °C per minute by employing alumina as a reference standard in a differential scanning calorimeter [28].

Photomicroscopy

A droplet was covered with a cover slip and set on a slide after the formed complex was suspended in distilled water. The photomicrographs were obtained using a microscope (Model: DM 2500, Leica Microsystems, Germany) under 20X magnification. The study was conducted using an optical microscope equipped with a camera [37].

Transmission Electron Microscopy (TEM)

A TECNAI 12 G2 TEM was used for the TEM analysis, a versatile 120 kV TEM suitable for all samples. Surface morphology was determined using TEM. A dilution of 20 µL of the sample in 6 mL distilled water was made, and 2 µL of the sample was coated on a copper-carbon grid and dried under an IR lamp for 5 min. Negative staining was performed with phosphotungstic acid, dried and analysed under TEM [37, 38].

In Vitro Drug Release Study

The *in vitro* drug release was carried out using the dialysis bag technique. To eliminate preservatives, distilled water was used to soak the dialysis membrane at room temperature, rinsed with distilled water once more, and then soaked in phosphate buffer saline (PBS) of pH 7.4. A dialysis bag (dialysis membrane-110, molecular weight cut off 12000) was filled with 1 mL of DL-UMB-CDLP suspension, equivalent to 10 mg of the drug. The bag was then hermetically sealed and submerged in 50 mL of PBS (pH 7.4) and ethanol in a 4:1 ratio. Using a magnetic stirrer, the medium was continuously stirred at 150 rpm while maintaining a temperature of 37 ± 0.5 °C and replacing a 5 mL sample at specified intervals to maintain the sink condition. UV spectrophotometric analysis using a UV-visible spectrophotometer (Shimadzu, UV-2700) at 324.5 nm measured the released drug. Lastly, Zero order, First order, Higuchi's equation, and Peppas-Korsmeyer four models were employed to evaluate the kinetics of the drug release [5].

Preparation of DL-UMB-CDLP Liposomal Gel

Four batches of the gel formulations were prepared by varying the concentration of Carbopol 934 from 1.0 %, 1.5 %, 2.0 % and 2.5 % for batch B1, B2, B3 and B4, respectively. Distilled water was used to soak the proper amount of Carbopol 934 for the entire night. In a beaker, 10 mL of distilled water was utilised to dissolve methyl and propylparaben (0.1 % and 0.01 %, respectively), and Carbopol 934P was added while being constantly stirred. The optimized formulation of DL-UMB-CDLP (1.0 %) was introduced into the mixture. Polyethylene glycol (PEG) 400 (2.5 %) was later added to the dispersion and mixed with triethanolamine to form a gel. Glass ointment bottles were used to hold the prepared gel, which was then kept at room temperature (Table S1 in the Supplementary Materials file) [37].

Evaluation of Gel

pH, Visual Inspection, Homogeneity and Grittiness

The pH of each gel was measured using a pH meter. The results were recorded after two minutes of dipping the electrode in a gel at 27 °C [39]. Visual assessments were conducted on all prepared gel batches to assess their organoleptic qualities, such as color, texture, consistency, and physical appearance [40]. Every gel formulation was tested by rubbing a tiny amount of the gel on the back of the hand and pressing it between the thumb and index finger [41]. Every batch of prepared gel was examined under a microscope to check for the presence of particles [42].

In Vitro Diffusion Study of Gel

The Franz-diffusion cells were used in the *in vitro* release investigation. The dialysis membrane was immersed in phosphate buffer (pH:6.8) for the entire night. 1g of gel was applied to the donor compartment, and 50 mL of phosphate buffer pH 6.8 was added to the receptor compartment. To maintain homogeneity, the mixture was constantly stirred at 150 rpm using a magnetic stirrer at 37 ± 0.5 °C and replenished with a 5 mL sample with an equal amount of freshly prepared buffer to maintain the sink condition, followed by spectrophotometric analysis at 324.5 nm [37].

Stability Studies

Stability assessments in this study were conducted at 4 °C ±1 °C / 45 %RH, room temperature (25 °C ± 1 °C /65 %RH), and 40 °C ± 1 °C /75 %RH for a specified duration ranging from 0 days to 30 days to 90 days for the optimized formulations. The liposomal suspension was stored in 20 mL sealed vials. Periodically, samples were taken out and examined for zeta potential, polydispersity index (PDI), and particle size. Analysis was done on the optimized DL-UMB-CDLP gel formulation's pH, drug content, drug release, and viscosity. ANOVA was used for statistical analysis and validation of this data [43].

Biological Evaluation

Animals

To evaluate the UV-protective properties of the double-loaded liposomal formulation as a gel, healthy Wistar rats weighing 150–200 g, both male and female, were acquired from the central animal house and housed under standard conditions (20–25 °C /55–65 % RH). During the seven days before the experiment, the rats were acclimated to their new surroundings in plastic cages with readily accessible water ad libitum and rat feed. They were also kept at the proper humidity and temperature. All the experiments were conducted per the Institutional Animal Ethical Committee's standard guidelines (Approval no. GCP/IAEC/2023/12) [25, 39].

Ex Vivo Skin Permeation

The rat skin was prepared for *ex vivo* permeation studies using a Franz diffusion cell (Perme Gear Standard Jacketed Franz cell USA) as per the reported method [25]. The rat skin was placed on the Franz diffusion cell in the proper orientation, with the dermal side confronting the receptor compartment filled with buffer and the stratum corneum side towards the donor compartment. Using a magnetic stirrer, the cell was continuously stirred at 37 ± 0.5 °C. Following that, 1 mL of the optimized DL-UMB-CDLP gel preparation and the standard UMB gel (0.1 %) that had been prepared in a similar way were applied evenly to the skin in the donor compartment. After specified intervals, 1 mL sample was withdrawn from the receptor compartment by maintaining the sink condition and analysed spectrophotometrically at 324.5 nm. A comparison was made between the double-loaded liposomal gel's skin penetration and the plain gel [25, 30].

Primary Skin Irritation Studies

Wistar albino rats ($n = 6$) were used in the skin irritation investigation of the prepared formulation. A 4 cm^2 area was marked after each rat's back hairs were clipped off with a trimmer. Rats ($n = 6$) were allocated at random to one of three categories: Group I: Control (received no drug in gel base), Group II: received UMB treatment in gel base and Group III: treated with optimized DL-UMB-CDLP loaded gel. The control and gel formulations were used for seven days in a row. Before administering each dose, the rat skin was cleansed, and for seven days, it was observed for any reactions, including erythema and edema [39, 44, 45].

Assessment of the Photoprotective Capacity of the Optimized DL-UMB-CDLP Gel Against UV Exposure

The UV lamp (Philips, India; TL 128 W, 315–400 nm; peak radiation at 370 nm) was used. A trimmer shaved a defined region on the rat's dorsal surface (2×3 cm^2). To find and eliminate rats exhibiting aberrant hair growth or a reaction to depilation, the rats were monitored for 48 h. Rats in this study were exposed to UVA for 20 min (610 mJ/cm^2; 4.42 times MED).

The experimental rats were divided into six groups (G1–G6). The rats' marked shaved area was covered with a thin, even layer of gel formulation. Animals in the control (G1) and UVA-irradiated (G2) groups received a placebo gel formulation. The UMB1 (G3) and UMB2 (G4) groups were given a standard UMB gel that contained 0.1 % medication. DL-UMB-CDLP gel, which includes a liposomal formulation equal to 0.1 % drug, was applied to the DL-UMB-CDLP1 (G5) and DL-UMB-CDLP2 (G6) groups. After topical application, the UVA-irradiated, UMB1 and DL-UMB-CDLP1 groups were immediately exposed to UV radiation for seven consecutive days. Following a 4 hours topical treatment, the G4 and G6 groups were subjected to UV light for 7 days (Table S2 of the Supplementary Materials file). All the rats were sacrificed using the cervical dislocation method on the eighth day. The skin's UV-exposed area was quickly removed in ice-cold saline, followed by homogenate preparation at 0.1 M PBS (pH 7.4) [25].

Estimation of Antioxidant Marker Enzymes in Cutaneous Tissue

The rat skin (2×3 cm^2) was cleaned in ice cold saline and sliced into small pieces, followed by immediate homogenisation. Further, a 10 % w/v skin tissue homogenate supernatant was obtained by centrifugation and assayed using kits of Elabscience US per reported methods for the estimation of the antioxidant marker enzymes reduced glutathione (GSH), superoxide dismutase (SOD), thiobarbituric acid reactants (TBARS), lipid peroxidation (LPO) and catalase (CAT) [24, 25].

Statistical Analysis

Except for the estimation of antioxidant enzyme levels in rat skin, which was done using mean ± standard error of means (SEM), all data were presented as mean ± standard deviation (SD). GraphPad Prism software was used to conduct the statistical analysis, using a one-way analysis of variance (ANOVA) and Dunnett's post hoc test. The mean differences were deemed significant when the p-value was less than 0.05.

Skin Histopathology

After being fixed in 10 % buffered formalin, skin specimens were processed and paraffin-embedded. Additional paraffin sections (7 μm) were taken and analysed under a microscope after being stained with hematoxylin and eosin to check for skin tissue disfigurement during the experiment [46].

Results and Discussion

Percent Yield

The percent yield of an inclusion complex is a useful metric for evaluating the efficiency of the preparation method and the strength of the host-guest interaction. Table S3 of the Supplementary Materials file displays the findings of the percent practical yield studies. It was found that the prepared inclusion complex's

practical yield ranged between 86.67 ±0.14 and 95.65 ±0.58 %. In **C5**, a higher yield for the UMB inclusion complex was demonstrated using the kneading method in a 1:2 ratio. The technique used to prepare molecular inclusion complexes is reproducible, as evidenced by low coefficient of variance (CV) values (<1.0 %) in the percentage yield [47].

Assay or Drug Content Estimation

Determining the amount of drug present in an inclusion complex through assay or drug content estimation is essential for comprehending its characteristics and uses. This is significant because the inclusion complex might exhibit different properties, like enhanced solubility or bioavailability, than the pure drug. All 12 formulations' actual drug contents are displayed in Table S3 of the Supplementary Materials file. It was discovered that the drug content of the prepared inclusion complex ranged from 77.37±0.64 to 98.34±0.40 %, demonstrating the use of current techniques to prepare inclusion complexes with high content uniformity. In **C5**, the highest percentage of drug content was discovered to be 98.34±0.40 %.

In Vitro Dissolution Studies

When a drug forms a complex with another molecule, such as cyclodextrin, *in vitro* dissolution studies of inclusion complexes measure how quickly the drug dissolves compared to the drug itself. These investigations aid to determine whether complexation speeds up the drug's rate of dissolution, which is critical to its efficacy and absorption. Inclusion complexes were prepared successfully, and the perfect combination for increasing the drug dissolution characteristics of the drug in comparison with its pure form was determined. Compared to pure drug, inclusion-complex drug release was faster. After 7 min, the cumulative percentage of drug released for **C5** was 98.9 ±0.13 %, whereas the cumulative percentage for pure drug UMB was 22.10 ±0.6 %. The dissolution rate of UMB from all inclusion complexes (apart from **C7** and **C10**) was significantly higher than that of pure UMB, according to the *in vitro* release study in Table S4 of the Supplementary Materials file.

According to the *in vitro* drug release profile, formulation **C5**, which contains HP-β-CD (1:2 ratio), exhibited a higher dissolution rate than the other formulations.

Characterisation of Optimized UMB Inclusion Complex

Saturation Solubility Studies

The solubility of optimized inclusion complex (**C5**) in PBS 7.4 was 33.04 mg/mL, which was approximately 6.5 times higher than pure drug UMB (5.09 mg/mL). UMB entrapment in the HP-β-CD cavity is one aspect of the host-guest interaction that may be responsible for the drug's increased solubility.

Fourier Transform Infrared Analysis (FT-IR)

IR studies are indicative of any interaction between ligand and guest molecules. FT-IR spectrum of optimized inclusion complex **C5** showed major peaks at 3315 cm^{-1} (O-H stretch) and 2922.60 cm^{-1} (C–H stretch) in which the hydroxyl group showed a broad peak along with the absence of the C=O group, indicating the formation of strong bonds between -OH group of HP-β-CD and drug in complex (Figure 1A).

DSC Analysis

It is an effective method for describing inclusion complexes, providing information on their properties and formation. The formation of a complex and the efficiency of the interaction between the host and guest molecules can be ascertained by examining the complex's thermal transitions. When the DSC thermogram of UMB is compared with that of the UMB inclusion complex (Figure 1B, 1C), it was observed that the thermogram of UMB inclusion complex showed a wide peak showing an endothermic peak at 82.68 °C and the endothermic peak at 123.13 °C corresponding to UMB was not visible indicating complete encapsulation of drug in HP-β-CD.

XRD Analysis

Understanding the structure and formation of an inclusion complex can be gained through XRD analysis. To ascertain the type of inclusion and validate the complex formation, researchers can compare the complex's diffraction patterns to those of the individual host and guest molecules. The XRD patterns of pure UMB and the **C5** are represented in Figures 1D and 1E. The XRD spectra of UMB showed strong reflections at around 11.7°, 15.97°, and 28°, indicating its crystalline nature. However, the peak intensities were somewhat diminished in the XRD spectrum of **C5**. The peak position (angle of diffraction) and the absence of separate, distinct peaks indicate the complex's amorphous nature. A diffractogram of the complex revealed the disappearance of most of the sharp peaks of the drug (crystalline nature), confirming complex formation with a greater amorphous nature of the inclusion complex than the free molecules [25].

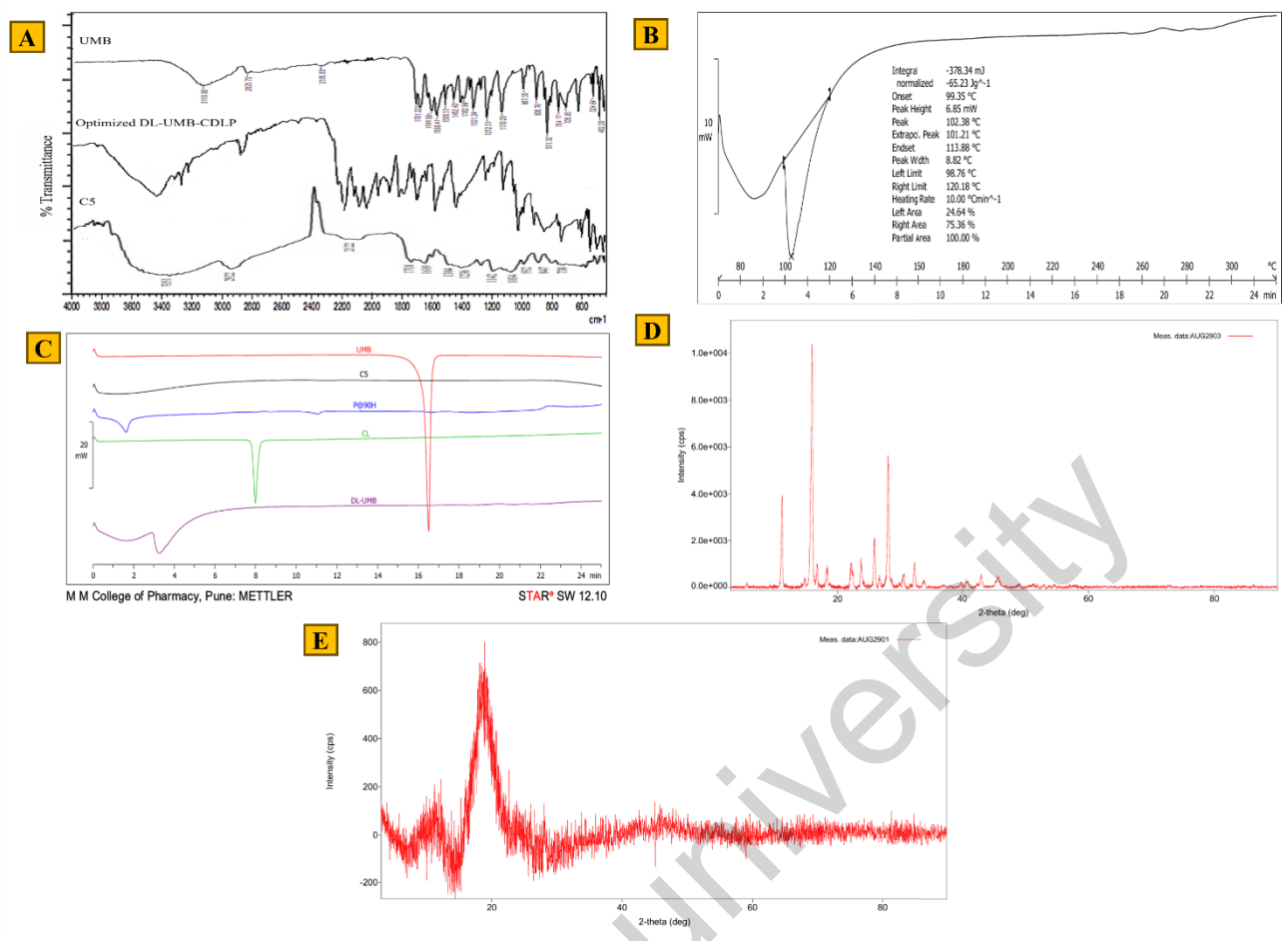

Figure 1. (*A*) FT-IR Spectra overlay of UMB, optimized batch of DL-UMB-CDLP and **C5**; (*B*) DSC thermograph of optimized DL-UMB-CDLP; (*C*) DSC thermograph overlay of UMB, **C5**, PL90H, Cholesterol and optimized DL-UMB-CDLP. (*D*, *E*) XRD diffractogram of UMB and **C5**

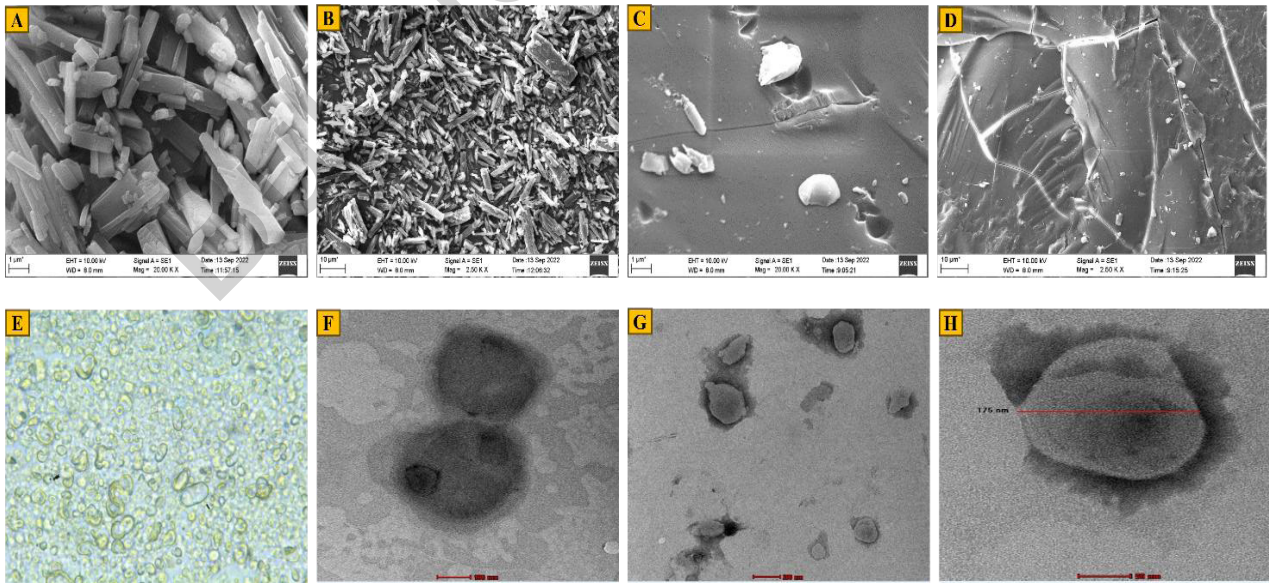

Figure 2. (*A*, *B*) SEM images of UMB at 20000× and 2500×. (*C*, *D*) SEM images of **C5** at 20000× and 2500×. (*E*) Microscopic image of the optimized DL-UMB-CDLP. (*F, G, H*) TEM images of optimized DL-UMB-CDLP

SEM

This method is applied to the analysis of the surface morphology of inclusion complexes. Observing changes in the particle morphology relative to the individual components makes it possible to ascertain whether the inclusion complex has been successfully formed. The SEM images of the pure drug UMB and **C5** at 20000× and 2500× magnification are depicted in Figure 2A–2D. UMB particles were observed to be crystalline individual particles, whereas the **C5** complex's irregular shape and rough surface morphology indicated complete conversion into a complex. The drug particles remained dispersed and physically adsorbed on the surface of HP-β-CD and showed homogeneity, signifying the inclusion of complex formation [32].

Formulation Development of DL-UMB-CDLP

The results shown in Table S5 of the Supplementary Materials file were obtained for the formulation development batch for 15 formulations of DL-UMB-CDLP. The batches prepared showed that factors such as PL90H : cholesterol ratio, Lipid : drug ratio and stirring speed significantly affected the formulated double-loaded liposomes' entrapment efficiency.

Use of Design of Experiments (DoE) for Process Optimisation

DoE is a structured and organised way to determine the relationship among various factors that effect the output of a process. A 3^3 factorial design was used to understand the effect of three independent variables: PL90H: cholesterol Ratio (A), Lipid: drug ratio (B), and stirring speed (C). Table S5 of the Supplementary Materials file lists the specifics of the 15 batches that were completed in triplicate. It was found that the vesicles' entrapment efficiency elevated as the PL90H: cholesterol ratio shifted from 5:5 to 7:3, and as the concentration of cholesterol increased, the vesicles' particle size reduced. Batches with the greatest PL90H: cholesterol ratio had greater entrapment efficiencies, whereas higher cholesterol levels caused lower entrapment. This may be because cholesterol in the lipid bilayer has displaced UMB [48].

Factorial Design for Entrapment Efficiency

The results show that the *p*-values of the model for entrapment efficiency were less than 0.001, indicating its significance. In this case, A, B, and C represented the formulation's constituent parts, and the equation showed how each of them quantitatively affected the variables. The following equation was obtained:

$$\%EE = 98.90 - 0.7400A - 0.3975B - 0.2025C - 0.5375AB - \\ - 1.99AC - 0.3025BC - 1.91A^2 + 0.6511B^2 - 2.75C^2$$

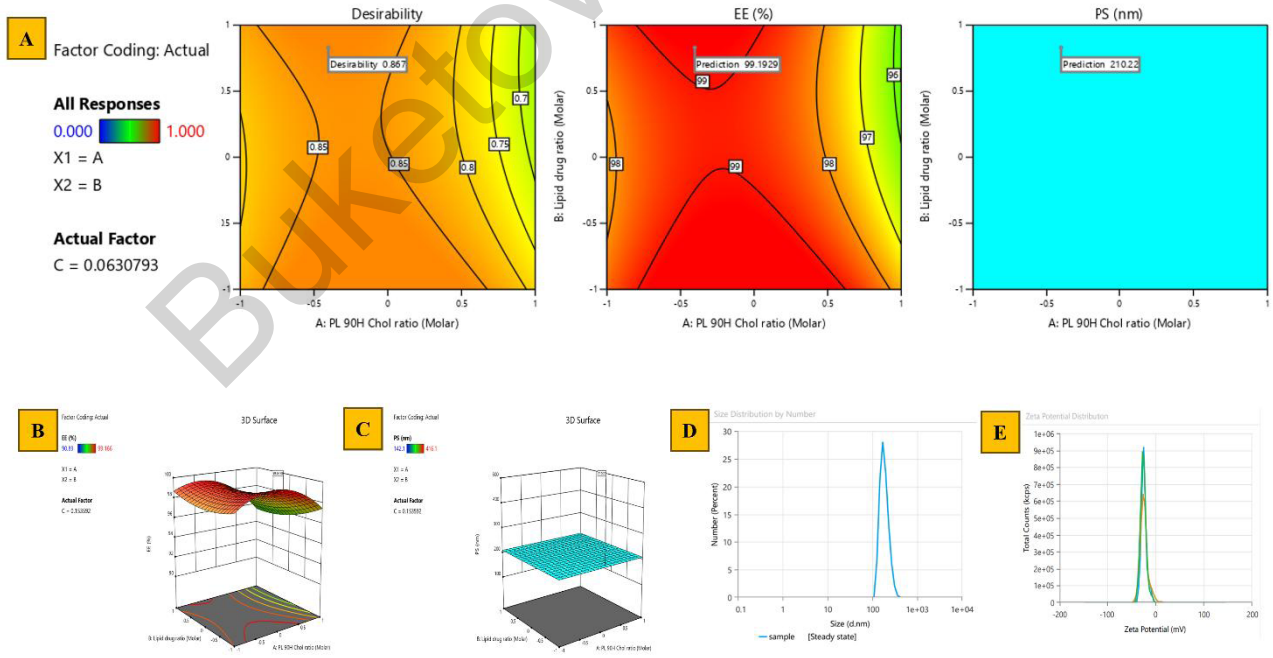

Figure 3. (*A*) The response surface plot and contour plots based on all the responses for DL-UMB-CDLP. (*B*, *C*) Contour plots based on the entrapment efficiency and particle size for DL-UMB-CDLP. (*D*, *E*) Particle size and zeta potential analysis of the optimized batch

According to the equation above, the PL90H: cholesterol concentration (A) had a positive coefficient, meaning it had a beneficial effect on the entrapment efficiency, whereas the concentration of cholesterol (B) had a negative coefficient, meaning it had a negative effect. *P* values of 0.05 indicate high significance of the regression coefficients. The contour plots shown in Figures 3A–3C schematically illustrates the response values. By altering the concentrations of the PL90H and cholesterol, these plots can be used to predict the system's entrapment efficiency.

Factorial Design for Particle Size

The results show that the model's p-value for particle size was 0.00004, indicating its significance.

Optimization

The formulation was optimized using the desirability function, taking into account PS at the minimum constraint and EE% at the maximum constraint. Numerical optimization predicted an optimal formulation with a lipid to drug ratio of 1.514:1, a PL90H to cholesterol ratio of 6.506:3.494, and a stirring speed of 813.8 rpm (coded values). The anticipated results were a particle size (PS) of 210.22 ±0.28 nm and an entrapment efficiency (EE) of 99.19 % ±0.39, with a corresponding desirability of 0.867. The improved formulation was created empirically to validate the model. The measured PS and EE values were 215.45 ±0.42 nm and 98.75 ±0.31 %, respectively. The percentage bias for PS and EE was determined to be 2.49 % for PS and 0.51 % for EE. These results confirm that the experimental values closely match the predicted outcomes with minimal bias, indicating the adequacy and reliability of the optimization model.

The optimized batch was DL-UMB-CDLP with a entrapment efficiency of 98.75 % ± 0.31 %, indicating successful entrapment of UMB into vesicles and a particle size of 215.45 ± 0.42 nm.

Evaluation of the optimized DL-UMB-CDLP Formulation

Zeta Potential Analysis

Zeta potential is another crucial metric frequently used to evaluate the liposomes' stability. The specificity and particle size distribution proved that the preparation method offers good homogeneity to double-loaded nanoparticles, and PL90H concentration plays a crucial role in the stability of formulations. The zeta potential of optimized batch was found to be –23.6 ±0.49 mV. Thus, the liposomal formulation is considered stable, further restraining the charged particles' aggregation. The particle size and zeta potential analysis results of the optimized formulations of DL-UMB-CDLP are depicted in Figures 3D and 3E.

A polydispersity index (PDI) value of the optimized DL-UMB-CDLP formulation was found to be 0.09±0.02, confirming monodisperse particles with better homogeneity. Lower PDI values show a better particle size homogeneity.

DSC Analysis

The DSC thermogram of UMB was compared with that of double-loaded liposomal formulations. The optimized formulation of DL-UMB-CDLP thermogram exhibits a single peak at 102.38 °C, which differs from the UMB peak. It is evident that the initially observed UMB peak vanishes from the thermogram of the corresponding liposomal formulation, and the endotherm is seen to be broadened and slightly shifted to a lower temperature. Thus, it can confirm that the liposomal formulation is formed.

Photomicroscopy

This analysis provides a powerful toolkit for visualizing and characterizing double-loaded liposomes. The microscopic images showed the presence of spherical structures of the complex. Figure 2E represents that liposomes are circular or slightly off-circular, with relatively thick edges. Lipid vesicles can be created without cholesterol, but the formed structures will be destroyed easily. Thus, it is quite clear from the images that cholesterol stabilizes the PL90H layers in the liposomes.

TEM

TEM analysis is used to visualise the morphology and size of double-loaded liposomes, revealing their spherical shape and variations in size. Since TEM analysis had a high spatial and atomic resolution, it was utilized to ascertain the internal and structural characteristics. The TEM verified the presence of spherical liposome vesicles (Figure 2F–2H). TEM analysis disclosed the development of homogenous unilamellar, discrete and almost spherical structures of liposomes [49].

In Vitro Drug Release Study

These studies seek to determine the overall effectiveness of the liposomal system, comprehend the release profile of the medications, and evaluate the effect of formulation on drug release kinetics. The drug

release plays a vital role in drug performance. The *in vitro* drug release study of UMB liposomes was carried out in a 4:1 ratio of PBS 7.4: Ethanol at 37 °C using the dialysis method. The release study was carried out for 5 hours. The release rate of the DL-UMB-CDLP was significantly different ($p < 0.05$) compared to UMB. The release profile of free UMB showed 59.65 ±1.04 % after 5 hours. The release profile of UMB formulations showed 81.64±10.6 % after 5 hours (Figure 4A). The release profile of the liposomal suspension showed a biphasic response with a comparatively significant burst effect followed by a slower release rate. This burst effect and its rate vary depending on the type of liposome and lipid concentration. Sometimes, the addition of cholesterol reduces the initial release rate. Our observation of the sustained manner of drug release is due to the phospholipid complex's slow drug diffusion [50, 51, 52].

Evaluation of Gel

pH, Visual Inspection, Homogeneity, Grittiness

Gel evaluation ensures these formulations' safety, efficacy, and quality, affecting their effectiveness and patient acceptability. Each prepared topical gel formulation ranged between 6.5 and 6.8 (Table S6 of the Supplementary Materials file), a safe range to apply to the skin. The color, texture, consistency, and appearance of the prepared gel formulations were visually inspected. Every prepared formulation had a smooth, viscous texture and a buff color. There was no alteration in the toughness of formulation for all the prepared formulations during application to the skin. No grainy particles and lumps were observed on the slide under microscopic examination.

In Vitro Diffusion Study of Gel

This study gives researchers a better understanding of how a drug will act in the body by simulating drug release and penetration through a barrier, such as the skin, under carefully monitored conditions. This aids in developing and optimising topical gels and other drug delivery systems for increased safety and effectiveness. *In vitro* release profile of optimized DL-UMB-CDLP loaded gels containing different concentrations of Carbopol is shown in Figure 4B; the cumulative release of the control gel was found to be 56.16±0.64 % at the end of 24 hours. Meanwhile, in the liposomal gel, B1, B2, B3, and B4 were found to be 86.29±1.04 %, s118.18±0.77 %, 104.47±0.76 % and 77.23±1.18 %, respectively. A significant difference ($p < 0.05$) was observed between the drug release retardation shown by UMB loaded gel and optimized DL-UMB-CDLP loaded gels. Since formulation B2 demonstrated the highest percentage of cumulative drug release, it was selected as the most optimal.

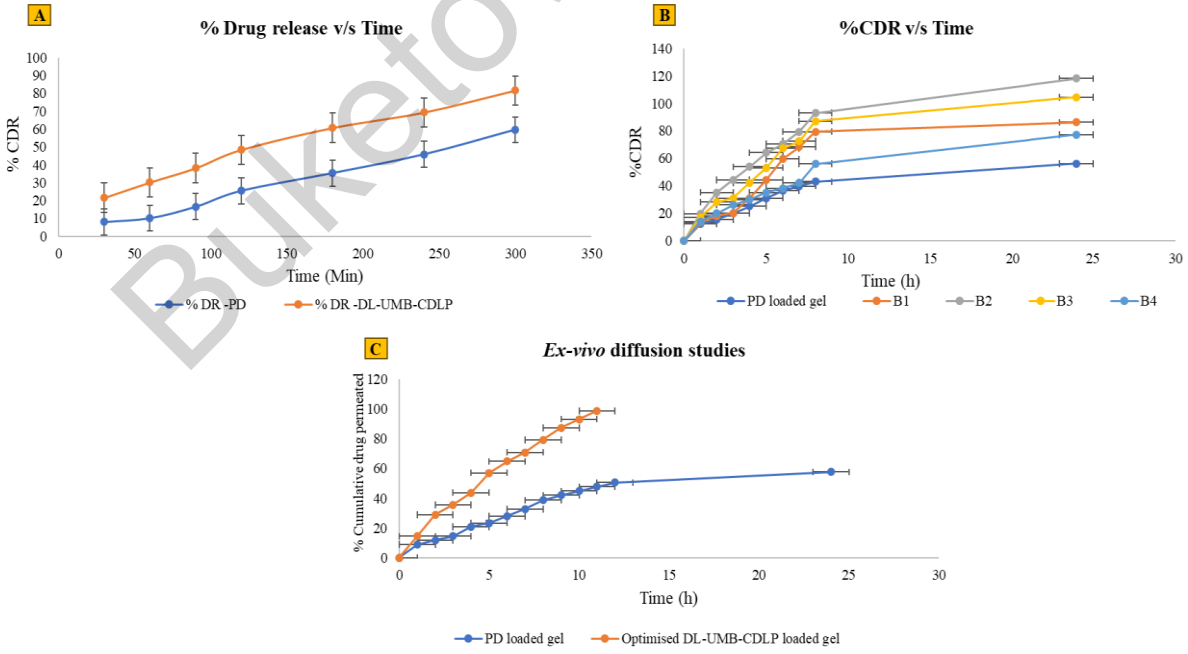

Figure 4. (A) *In vitro* drug release profile of pure drug UMB and optimized DL-UMB-CDLP. (B) *In vitro* drug diffusion profile of optimized DL-UMB-CDLP loaded gel. (C) Graphical representation of % cumulative drug permeation of optimized DL-UMB-CDLP loaded gel formulation and UMB loaded gel using rat skin

Kinetic Modelling of Optimized Gel

Model fitting of the permeation profile of drug from the UMB loaded gel and optimized DL-UMB-CDLP loaded gel was performed using Zero order, First order, Higuchi and Korsmeyer–Peppas models, which exhibited R^2 values of 0.9933, 0.8199, 0.9793 and 0.9962, respectively. Based on the highest coefficient of correlation, the best fit was shown by Korsmeyer–Peppas model ($R^2 = 0.9962$) and the value of permeation coefficient (n) for the drug and complex was obtained to be $0.5 < n < 1$. This indicates a non-Fickian pattern of drug release, i.e. a combination of drug diffusion and matrix erosion. The simple Korsmeyer-Peppas model describes drug release from a polymeric system, also called the "Power law". Some release mechanisms, including the diffusion of the vehicle into the matrix, the matrix's swelling, and the matrix's dissolution, are simultaneously described by the Korsmeyer-Peppas model. The developed liposomal gel has a dual action: ethanol causes skin disruption, and the vesicle action leads to the drug release [31].

Stability Study

Stability study assesses how a pharmaceutical formulation's efficacy, safety, and quality are preserved over time under various handling and storage conditions. Determining the product's shelf life, ideal storage conditions, and suitable packaging is an essential step in the process. The study helps ensure that the medication will maintain its potency, purity, and other quality characteristics throughout its anticipated use. The stability studies of the optimum formulation showed that the liposomal formulation's drug content and entrapment efficiency did not significantly decrease over 30 and 90 days. The results are shown in Tables S7 and S8 of the Supplementary Materials file. Changes in pH were noted, which slightly reduced with time. Maximum changes were observed in formulations stored at room temperature and 40 ˚C. Therefore, the formulations can be stored at 4 ˚C.

Biological Evaluation

Ex Vivo Skin Permeation Studies

These studies are crucial for understanding drug delivery, evaluating the efficacy of formulations, and predicting how substances will interact with the skin. The comparative results of the cumulative release percentage of the pure drug UMB-loaded gel and the optimized DL-UMB-CDLP gel through the skin are shown in Figure 4C. The cumulative release of the pure drug UMB-loaded gel was 57.76 ±0.56 % at the end of 24 hours. Meanwhile, in DL-UMB-CDLP gel, the cumulative release was 98.76 ±0.94 % at the end of 11 hours. When comparing the optimized DL-UMB-CDLP gel to the traditional UMB-loaded gel, the drug release value after 24 hours was significantly higher ($p < 0.05$), indicating a notable improvement in release rate. The presence of phospholipid constituents, which altered the skin layer and improved drug penetration, may have contributed to the enhanced penetration of the optimized DL-UMB-CDLP gel. In contrast, this type of interaction was absent from the conventional UMB-loaded gel. The prepared optimized DL-UMB-CDLP gel was better at facilitating drug penetration and sustained release of UMB, according to this *ex vivo* study conducted for 24 hours [53].

Primary Skin Irritation Studies

This test is crucial for determining the potential of a substance to cause irritation or damage to the skin. The prepared gel formulation was found safe when its skin-irritating effect was assessed. No erythema or edema was seen in any formulation after seven days of study. Additionally, the finer gel matrix mesh of Carbopol 934P prevents droplets from penetrating into the deeper layers of the skin, reducing skin irritation.

Histopathological Analysis of the Skin for Skin Irritancy Testing

A skin irritancy test was done to check vehicle compatibility with the skin and confirm if the DL-UMB-CDLP gel formulation caused any dose toxicity. Figure 5A–5C displays the findings of the skin's histopathological examination. In this group, 2 (G2), a plain drug-loaded gel, showed mild dermal congestion and inflammatory infiltration. In contrast, gel vehicle (G1) and the optimized gel formulation (G3) showed no histological changes in the skin. Microscopic images show that the vehicle gel base (G1) and the DL-UMB-CDLP gel (G3) are compatible with skin as they do not cause any epidermal changes in the rat skin.

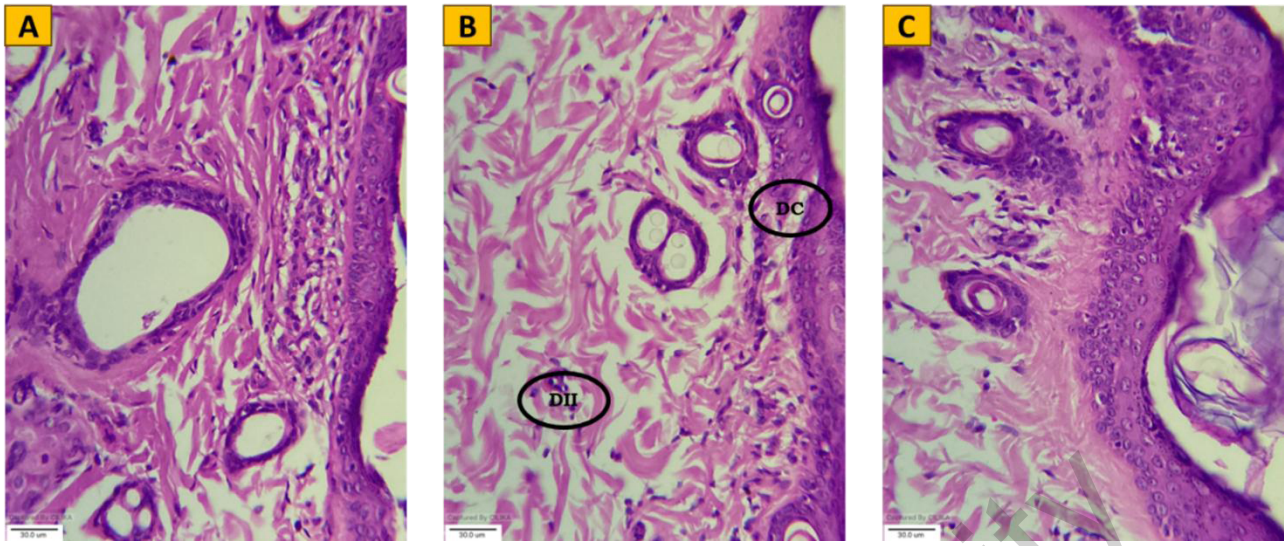

Legend on the figure Bn: (DC) — Microscopy-Dermal Congestion, (DII) — Dermal Inflammatory Infiltratio

Figure 5. Photomicrographs of histological sections of the rat skin for skin irritancy testing.
(A) G1 — Gel base. (B) G2 — Placebo. (C) G3 — Optimized DL-UMB-CDLP loaded gel

Assessment of the Photoprotective Capacity of the Optimized DL-UMB-CDLP Gel Against UV Exposure

Rats that underwent this procedure but did not receive UMB treatment (G2 group) exhibited oxidative damage due to the UV irradiation model we used in our study. Decreased activity of CAT, GSH, and SOD indicates depletion of the endogenous antioxidant system, and an increase in the TBARS marker, a marker that sets the lipid peroxidation index, was used to confirm oxidative damage (Figure 6). The effects on individual markers in different groups are depicted in Figure S3 of the Supplementary Materials file. CAT, GSH, and SOD activities significantly recovered in animals that were exposed to the same irradiation protocol and received immediate UV treatment following the application of DL-UMB-CDLP gel formulation. These animals also showed no signs of lipid peroxidation (low TBARS value), comparable to the outcomes of the non-irradiated control (G1) group. These findings demonstrated the UMB's ability to protect against oxidative damage caused by UV radiation and are associated with its antioxidant activity, which has already been elucidated in previous studies [24, 54, 55].

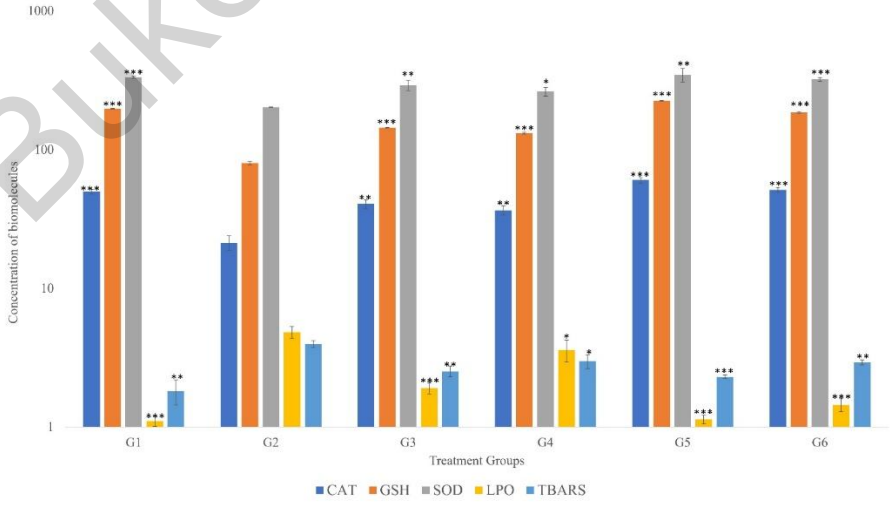

Figure 6. Effect of UV exposure on the antioxidant enzymes CAT, GSH, SOD, LPO and TBARS
One-way ANOVA followed by Dunnett's post hoc test.
Data represents mean±SD. (n = 6), *p < 0.01, **p < 0.001, and.***p < 0.0001 vs G2

Histopathological Analysis of the Skin for Photoprotective Activity

Skin histopathological analysis is important for assessing photoprotective activity because it allows researchers to determine how UV radiation and protective agents affect the cellular and structural integrity of the skin. This analysis helps determine whether a substance or product can reduce or prevent the harmful effects of UV radiation on the skin. The microscopic images are shown in Figure 7. The histopathological analysis of the skin in the UV irradiated control group (G2) showed mild dermal congestion, stratum corneum degeneration, fibrosis and dermal inflammatory infiltration. Fibrosis and hyperkeratosis were observed in the UMB 1 gel group (G3), whereas the UMB 2 gel group (G4) showed stratum corneum degeneration. This study indicates that the vehicle gel base is compatible with the skin, and the DL-UMB-CDLP gel (with immediate UV exposure) did not cause any epidermal changes in the rat skin compared to the UV-irradiated control group [14].

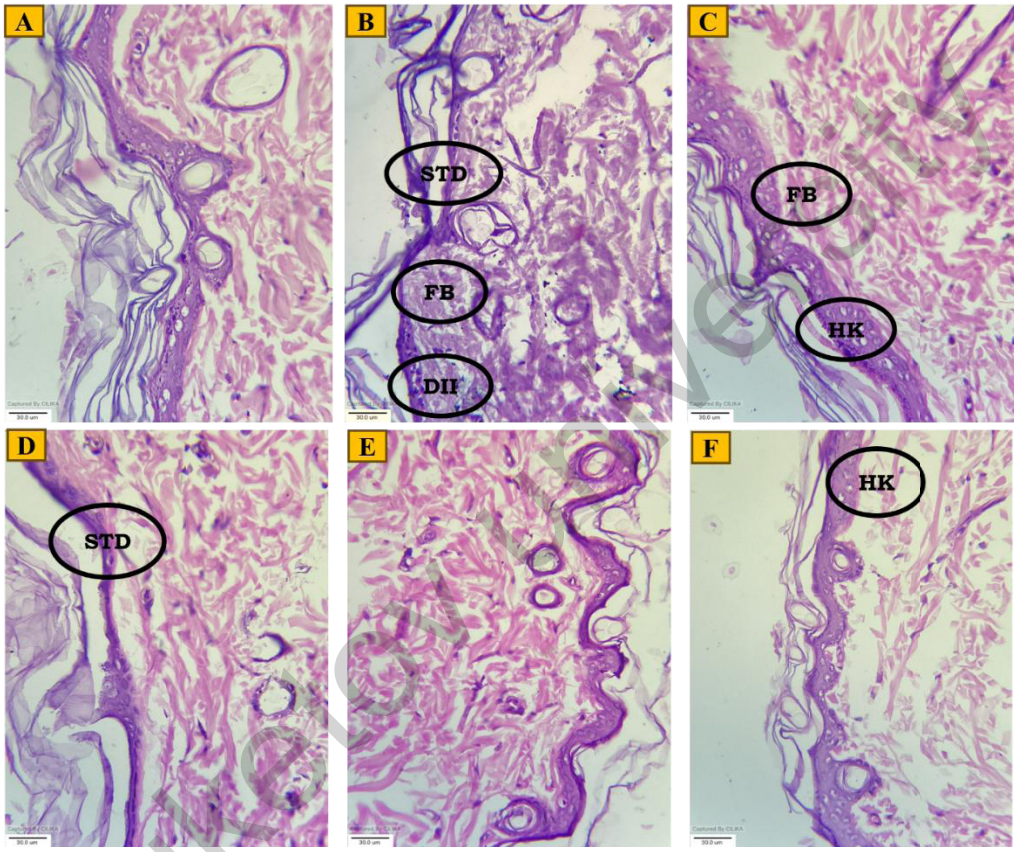

Legend on the microscopy figures: (DC) Dermal Congestion, (DII) Dermal inflammatory infiltration, (STD) Stratum corneum degeneration, (FB) Fibrosis, (HK) Hyperkeratosis

Figure 7. Photomicrographs of histological sections of the rat skin for photoprotective activity: (A) G1-Gel base; (B) G2- UV Irradiated control; (C) G3- UMB 1 gel; (D) G4- UMB 2 gel; (E) G5- DL-UMB-CDLP 1 gel; (F) G6- DL-UMB-CDLP 2 gel

Conclusions

The current work is a novel way to improve UMB's poor bioavailability and low aqueous solubility by complexing it with β-CD and then delivering the drug via liposomal delivery (DL-UMB-CDLP). The UMB-β-CD complex was successfully encapsulated in double-loaded liposomes using the thin-film hydration technique, PL90H, and cholesterol. The impact of independent variables on entrapment efficiency and particle size was examined using the 3^3 full factorial design. The research findings suggest that the DL-UMB-CDLP may be helpful for the sustained release of UMB, a poorly soluble drug. Additionally, it was concluded that the formulation may increase UMB's solubility and prolong its release for improved therapeutic efficacy. In conclusion, the optimized formulation DL-UMB-CDLP loaded gel presented physicochemical characteristics suitable for topical application and shielded the animal's skin from UVA and UVB radiation damage.

UMB's antioxidant and anti-inflammatory qualities and capacity to absorb UV radiation may be linked to the photoprotective effect.

Supporting Information

The Supporting Information is available free at https://ejc.buketov.edu.kz/index.php/ejc/article/view/341/227

*Author Information**

**The authors' names are presented in the following order: First Name, Middle Name and Last Name*

Rucheera Raju Verekar — PhD, Research Scholar, Goa College of Pharmacy, Goa University, 403001, Panaji, Goa, India; e-mail: rucheeraverekar@gmail.com; https://orcid.org/0000-0003-0197-3325

Shamshad Bi Mainoddin Shaikh — Assistant Professor, Zoology Discipline, School of Biological Sciences and Biotechnology, Goa University, 403206, Taleigao Plateau Goa, India; e-mail: shamshad.shaikh@unigoa.ac.in; https://orcid.org/0000-0001-8907-1398

Sarita Rebelo — PhD, Research Scholar, Zoology Discipline, School of Biological Sciences and Biotechnology, Goa University, 403206, Taleigao Plateau Goa, India; e-mail: zoology.sarita@unigoa.ac.in; https://orcid.org/0009-0008-1443-4383

Shailendra Shivaji Gurav (*corresponding author*) — Professor, Department of Pharmacognosy and Phytochemistry, Goa College of Pharmacy, Goa University, 403001, Panaji, Goa, India; e-mail: shailendra.gurav@nic.in; https://orcid.org/0000-0001-5564-2121

Author Contributions

The manuscript was written through contributions of all authors. All authors have given approval to the final version of the manuscript. CRediT: **Rucheera Raju Verekar:** Writing — Original draft preparation, Methodology, Software Data analysis; Resources; **Shamshad Bi Mainoddin Shaikh and Sarita Rebelo:** Writing — Review and editing, Methodology, Software Data analysis; Resources; **Shailendra Shivaji Gurav:** Conceptualisation, Methodology, Supervision, Investigation, Project Administration.

Acknowledgement

Authors are grateful to Dr. Madhusudan Joshi (Professor and Head of Pharmacology Department), of Goa College of Pharmacy, Government of Goa; Dr. S.C. Ghadi (Sr. Professor) and Dr. Nitin Sawant (Asst. Professor) of School of Biological Sciences and Biotechnology, Goa University, for providing the facilities to perform the research activities pertaining to animal studies.

Ethics approval and consent to participate

Animal experimentation procedures were followed per CPCSEA guidelines.

Conflicts of interest

The authors declare no conflict of interest.

References

1 Usapkar, P., Saoji, S., Jagtap, P., Ayyanar, M., Kalaskar, M., Gurav, N., & Gurav, S. (2024). QbD-guided phospholipid-tagged nanonized boswellic acid naturosomal delivery for effective rheumatoid arthritis treatment. *Int J Pharmaceutics: X*, 7, Art. 100257. https://doi.org/10.1016/j.ijpx.2024.100257

2 Fernández-Romero, A.M., Maestrelli, F., Mura, P.A., Rabasco, A.M., & González-Rodríguez, M.L. (2018). Novel findings about double-loaded Curcumin-in-HPβcyclodextrin-in liposomes: Effects on the lipid bilayer and drug release. *Pharmaceutics*, 10(4), 256. https://doi.org/10.3390/pharmaceutics10040256

3 Schnyder, A. & Huwyler, J. (2005). Drug transport to brain with targeted liposomes. *NeuroRX: The Journal of the American Society for Experimental NeuroTherapeutics*, 2(1), 99–107. https://doi.org/10.1602/neurorx.2.1.99

4 Brandl, M. (2001). Liposomes as drug carriers: a technological approach. *Biotechnology Annual Review*, 7, 59–85. https://doi.org/10.1016/s1387-2656(01)07033-8

5 Jhan, S. & Pethe, A.M. (2020). Double-loaded liposomes encapsulating lycopene β-cyclodextrin complexes: preparation, optimization, and evaluation. *J Liposome Res*, 30(1), 80–92. https://doi.org/10.1080/08982104.2019.1593450

6 Mccormack, B. & Gregoriadis, G. (1994). Drugs-in-cyclodextrins-in liposomes: a novel concept in drug delivery. *International Journal of Pharmaceutics*, 112, 249–258. https://doi.org/10.1016/0378-5173(94)90361-1

7 Gregoriadis, G. & Florence, A.T. (1993). Liposomes in drug delivery. Clinical, diagnostic and ophthalmic potential. *Drugs*, 45(1), 15–28. https://doi.org/10.2165/00003495-199345010-00003

8 Bhatt, P., Lalani, R., Vhora, I., Patil, S., Amrutiya, J., Misra, A., & Mashru, R. (2018). Liposomes encapsulating native and cyclodextrin enclosed paclitaxel: Enhanced loading efficiency and its pharmacokinetic evaluation. *International journal of pharmaceutics*, 536(1), 95–107. https://doi.org/10.1016/j.ijpharm.2017.11.048

9 Azzi, J., Jraij, A., Auezova, L., Fourmentin, S., & Greige-Gerges, H. (2018). Novel findings for quercetin encapsulation and preservation with cyclodextrins, liposomes, and drug-in-cyclodextrin-in-liposomes. *Food Hydrocolloids*, 81, 328–340. https://doi.org/10.1016/j.foodhyd.2018.03.006

10 Baccarin, T., Mitjans, M., Ramos, D., Lemos-Senna, E., & Vinardell, M.P. (2015). Photoprotection by Punica granatum seed oil nanoemulsion entrapping polyphenol-rich ethyl acetate fraction against UVB-induced DNA damage in human keratinocyte (HaCaT) cell line. *J Photochem Photobiol B*, 153, 127–136. https://doi.org/10.1016/j.jphotobiol.2015.09.005

11 Türker, H. (2015). The effect of ultraviolet radiation of pancreatic exocrine cells in mole rats: An ultrastructural study. *J Radiat Res Appl Sci*, 8(1), 49–54. http://dx.doi.org/10.1016/j.jrras.2014.10.006

12 Batista, C.M., Alves, A.V.F., Queiroz, L.A., Lima, B.S., Filho, R.N.P., Araújo, A.A.S., de Albuquerque Júnior, R.L.C., & Cardoso, J.C. (2018). The photoprotective and anti-inflammatory activity of red propolis extract in rats. *J Photochem Photobiol B*, 180, 198–207. https://doi.org/10.1016/j.jphotobiol.2018.01.028

13 Gu, Y., Han, J., Jiang, C., & Zhang, Y. (2020). Biomarkers, oxidative stress and autophagy in skin aging. *Ageing Research Reviews*, 59, Art. 101036. https://doi.org/10.1016/j.arr.2020.101036

14 Serafini, M.R., Detoni, C.B., Menezes, P.D.P., Pereira Filho, R.N., Fortes, V.S., Vieira, M.J.F., Guterres, S.S., Cavalcanti de Albuquerque Junior, R.L., & Araujo, A.A.S. (2014). UVA-UVB photoprotective activity of topical formulations containing morinda citrifolia extract. *Biomed Res Int*, Art. 587819. http://dx.doi.org/10.1155/2014/587819

15 Nobile, V., Michelotti, A., Cestone, E., Caturla, N., Castillo, J.O., Benavente-García, Pérez-Sánchez, A., & Micol, V. (2016). Skin photoprotective and antiageing effects of a combination of rosemary (Rosmarinus officinalis) and grapefruit (Citrus paradisi) polyphenols. *Food Nutr Res*, 60. http://dx.doi.org/10.3402/fnr.v60.31871

16 Liu, X., Zhang, R., Shi, H., Li, X., Li, Y., Taha, A., & Xu, C. (2018). Protective effect of curcumin against ultraviolet A irradiation-induced photoaging in human dermal fibroblasts. *Mol Med Rep*, 17(5), 7227–7237. https://doi.org/10.3892/mmr.2018.8791

17 Zhou, Y., Yang, W., Li, Z., Luo, D., Li, W., Zhang, Y., Wang, X., Fang, M., Chen, Q., & Jin, X. (2018). Moringa oleifera stem extract protect skin keratinocytes against oxidative stress injury by enhancement of antioxidant defense systems and activation of PPARα. *Biomedicine and Pharmacotherapy*, 107, 44–53. https://doi.org/10.1016/j.biopha.2018.07.152

18 Cho, B.O., Che, D.N., Shin, J.Y., Kang, H.J., Kim, J.H., Kim, H.Y., Cho, W.G., & Jang, S.I. (2017). Ameliorative effects of Diospyros lotus leaf extract against UVB-induced skin damage in BALB/c mice. *Biomedicine and Pharmacotherapy*, 95, 264–274. http://dx.doi.org/10.1016/j.biopha.2017.07.159

19 Nery, E.M., Martinez, R.M., Velasco, M.V.R., & Baby, A.R. (2020). A short review of alternative ingredients and technologies of inorganic UV filters. *J Cosmet Dermatol*, 00, 1–5. https://doi.org/10.1111/jocd.13694

20 Schneider, S.L. & Lim, H.W. (2019). A review of inorganic UV filters zinc oxide and titanium dioxide. *Photodermatol Photoimmunol Photomed*, 35, 442–446. https://doi.org/10.1111/phpp.12439

21 Schneider, S.L. & Lim, H.W. (2019). Review of environmental effects of oxybenzone and other sunscreen active ingredients. *J Am Acad Dermatol*, 80(1), 266–271. https://doi.org/10.1016/j.jaad.2018.06.033

22 Narla, S. & Lim, H.W. (2020). Sunscreen: FDA regulation, and environmental and health impact. *Photochem Photobiol Sci*, 19, 66–70. https://doi.org/10.1039/C9PP00366E

23 Kullavanijaya, P. & Lim, H.W. (2005). Photoprotection. *J Am Acad Dermatol*, 52(6), 937–958. https://doi.org/10.1016/j.jaad.2004.07.063

24 de Araújo, A.T., Heimfarth, L., dos Santos, D.M., dos Santos, M.R.V., de Albuquerque-Júnior, R.L.C., dos Santos-Neto, A.G., de Araujo, G.R.S., Lira, A.A.M., Matos, S.S., Frank, L.A., Rabelo, T.K., Quintans-Júnior, L.J., de Souza Siqueira Quintans, J., de Souza Araujo, A.A., & Serafini, M.R. (2022). Hesperetin-based hydrogels protect the skin against uv radiation-induced damage. *AAPS PharmSciTech*, 23(6), 170. https://doi.org/10.1208/s12249-022-02323-8

25 Ittadwar, P.A. & Puranik, P.K. (2016). Novel umbelliferone phytosomes: development and optimization using experimental design approach and evaluation of photoprotective and antioxidant activity. *Int J Pharm Pharm Sci*, 9(1), 218–228. http://dx.doi.org/10.22159/ijpps.2017v9i1.14635

26 Bhargava, S. & Agrawal, G.P. (2008). Preparation & characterization of solid inclusion complex of cefpodoxime proxetil with beta-cyclodextrin. *Current Drug Delivery*, 5(1), 01–06. http://dx.doi.org/10.2174/156720108783330998

27 Cid-Samamed, A., Rakmai, J., Mejuto, J.C., Simal-Gandara, J., & Astray, G. (2022). Cyclodextrins inclusion complex: Preparation methods, analytical techniques and food industry applications. *Food Chemistry*, 384, Art. 132467. https://doi.org/10.1016/j.foodchem.2022.132467

28 Darekar, T., Aithal, K.S., Shirodkar, R., Kumar, L., Attari, Z., & Lewis, S. (2016). Characterization and *in-vivo* evaluation of lacidipine inclusion complexes with β-cyclodextrin and its derivatives. *J Incl Phenom Macrocycl Chem*, 84, 225–235. https://doi.org/10.1007/s10847-016-0600-9

29 Tan, Q., Liu, S., Chen, X., Wu, M., Wang, H., Yin, H., He, D., Xiong, H., & Zhang, J. (2012). Design and evaluation of a novel evodiamine-phospholipid complex for improved oral bioavailability. *AAPS PharmSciTech*, 13(2), 534–547. https://doi.org/10.1208/s12249-012-9772-9

30 Bhattacharyya, S., Majhi, S., Saha, B.P., & Mukherjee, P.K. (2014). Chlorogenic acid-phospholipid complex improve protection against UVA induced oxidative stress. *J Photochem Photobiol B*, 130, 293–298. http://dx.doi.org/10.1016/j.jphotobiol.2013.11.020

31 Gurav, S., Usapkar, P., Gurav, N., Nadaf, S., Ayyanar, M., Verekar, R., & Chikhale, R. (2022). Preparation, characterization, and evaluation (in-vitro, ex-vivo, and in-vivo) of naturosomal nanocarriers for enhanced delivery and therapeutic efficacy of hesperetin. *Plos one*, 17(11), e0274916. https://doi.org/10.1371/journal.pone.0274916

32 Sapana, B.B. & Shashikant, D.N. (2015). Preparation and characterisation of β-cyclodextrin nebivolol inclusion complex. *Int J Pharm Sci Res*, 6(5), 2205. http://dx.doi.org/10.13040/IJPSR.0975-8232.6

33 Yue, P.F., Yuan, H.L., Li, X.Y., Yang, M., & Zhu, W.F. (2010). Process optimization, characterization and evaluation *in-vivo* of oxymatrine-phospholipid complex. *Int J Pharm*, 387(1–2), 139–146. https://doi.org/10.1016/j.ijpharm.2009.12.008

34 Soni, G. & Yadav, K.S. (2014). High encapsulation efficiency of poloxamer-based injectable thermoresponsive hydrogels of etoposide. *Pharm Dev Technol*, 19(6), 651–661. https://doi.org/10.3109/10837450.2013.819014

35 Galiyeva, A.R., Tazhbayev, Ye.M., Zhumagaliyeva, T.S., Sadyrbekov, D.T., Kaikenov, D.A., Karimova, B.N., & Shokenova, S.S. (2022). Polylactide-co-glycolide nanoparticles immobilized with isoniazid: Optimization using the experimental Taguchi method. *Bulletin of the University of Karaganda — Chemistry*, 105(1), 69–77. https://doi.org/10.31489/2022Ch1/69-77

36 Saoji, S.D., Rarokar, N.R., Dhore, P.W., Dube, S.O., Gurav, N.S., Gurav, S.S., & Raut, N.A. (2022). Phospholipid based colloidal nanocarriers for enhanced solubility and therapeutic efficacy of withanolides. *J Drug Deliv Sci Technol*, 70, 103251. https://doi.org/10.1016/j.jddst.2022.103251

37 Metkari, V., Shah, R., Salunkhe, N., & Gurav, S. (2023). QBD approach for the design, optimization, development, and characterization of Naringenin-loaded phytosomes to enhance solubility and oral bioavailability. *J Pharm Innovation*, 18(4), 2083–2097. https://doi.org/10.1007/s12247-023-09775-w

38 Gracias, S., Ayyanar, M., Peramaiyan, G., Kalaskar, M., Redasani, V., Gurav, N., & Gurav, S. (2023). Fabrication of chitosan nanocomposites loaded with biosynthetic metallic nanoparticles and their therapeutic investigation. *Environ Res*, 234, 116609. https://doi.org/10.1016/j.envres.2023.116609

39 Rodrigues, K., Nadaf, S., Rarokar, N., Gurav, N., Jagtap, P., Mali, P., Ayyanar, M., Kalaskar, M., & Gurav, S. (2022). QBD approach for the development of hesperetin loaded colloidal nanosponges for sustained delivery: *In-vitro, ex-vivo*, and *in-vivo* assessment. *OpenNano*, 7. https://doi.org/10.1016/j.onano.2022.100045

40 Aiyalu, R., Govindarjan, A., & Ramasamy, A. (2016). Formulation and evaluation of topical herbal gel for the treatment of arthritis in animal model. *Brazilian Journal of Pharmaceutical Sciences*, 52(3), 493–507. http://dx.doi.org/10.1590/S1984-82502016000300015

41 Chen, M.X., Alexander, K.S., & Baki, G. (2016). Formulation and evaluation of antibacterial creams and gels containing metal ions for topical application. *J Pharm*, 1–10. http://dx.doi.org/10.1155/2016/5754349

42 Opatha, S.A.T., Titapiwatanakun, V., Boonpisutinant, K., & Chutoprapat, R. (2022). Preparation, characterization and permeation study of topical gel loaded with transfersomes containing asiatic acid. *Molecules*, 27(15), 4865. https://doi.org/10.3390/molecules27154865

43 Wasankar, S., Wasankar, S.R., Faizi, S.M., & Deshmuk, A.D. (2012). Formulation and development of liposomal gel for topical drug delivery system. *IJPSR*, 3(11), 4461–4470. http://dx.doi.org/10.13040/IJPSR.0975-8232.3(11).4461-70

44 Wayal, S.R. & Gurav, S.S. (2021). Evaluation of wound healing potential of Bhallatakadi Ghrita — Cow ghee based polyherbal formulation: *In-vivo* excision and incision wound model. *J Complement Integr Med*, 18(3), 507–515. https://doi.org/10.1515/jcim-2020-0179

45 James, O. (2014). Evaluation of acute dermal irritation and wound contraction by Gymnema Sylvestre and Datura Metel extracts in rats. *American Journal of Biomedical and Life Sciences*, 2(4), 83–88. https://doi.org/10.11648/j.ajbls.20140204.14

46 Verekar, R.R., Gurav, S.S., & Bolmal, U. (2020). Thermosensitive mucoadhesive in situ gel for intranasal delivery of Almotriptan malate: Formulation, characterization, and evaluation. *J Drug Deliv Sci Technol*, 58. https://doi.org/10.1016/j.jddst.2020.101778

47 Dua, K., Pabreja, K., Ramana, M.V., & Lather, V. (2011). Dissolution behavior of β-cyclodextrin molecular inclusion complexes of aceclofena. *J Pharm Bioallied Sci*, 3(3), 417–425. https://doi.org/10.4103/0975-7406.84457

48 Yessentayeva, N.A., Galiyeva, A.R., Daribay, A.T., Sadyrbekov, D.T., Moustafine, R.I., & Tazhbayev, Y.M. (2024). Optimization of polylactide-co-glycolide-rifampicin nanoparticle synthesis, *in vitro* study of mucoadhesion and drug release. *Polymers*, 2024, 16, Art. 2466. https://doi.org/10.3390/polym16172466

49 Meister, A. & Blume, A. (2017). (Cryo) Transmission electron microscopy of phospholipid model membranes interacting with amphiphilic and polyphilic molecules. *Polymers*, 9, 521. https://doi.org/10.3390/polym9100521

50 Thippeswamy, B.S., Thakker, S.P., Tubachi, S., Kalyani, G.A., Netra, M.K., Patil, U., Desai, S., Gavimath, C.C., & Veerapur, V.P. (2009). Cardioprotective effect of cucumis trigonus roxb on isoproterenol-induced myocardial infarction in rat. *Am J Pharmacol Toxicol*, 4(2), 29–37. http://dx.doi.org/10.3844/ajptsp.2009.29.37

51 Mishra, R.K. & Singhal, G.S. (1990). Calcium and magnesium induced changes in the relative fluidity of phosphatidylcholine liposomes. *J Biosci*, 15(3), 193–197. https://doi.org/10.1007/BF02703884

52 Tazhbayev, Ye.M., Galiyeva, A.R., Zhumagaliyeva, T.S., Burkeyev, M.Zh., Kazhmuratova, A.T., Zhakupbekova, E.Zh., Zhaparova, L.Zh. & Bakibayev, A.A. (2021). Synthesis and characterization of isoniazid immobilized polylactide-co-glycolide nanoparticles. *Bulletin of the University of Karaganda — Chemistry*, 101(1), 61–70. https://doi.org/10.31489/2021Ch1/61-70

53 Shah, N. & Patel, K. (2023). Formulation, development and characterization of liposome-based gel of eberconazole nitrate for topical delivery. *Int J Pharm Investig*, 13(3), 485–495. https://doi.org/10.5530/ijpi.13.3.060

54 Bodduluru, L.N., Kasala, E.R., Barua, C.C., Karnam, K.C., Dahiya, V., & Ellutla. M. (2015). Antiproliferative and antioxidant potential of hesperetin against benzo(a)pyrene-induced lung carcinogenesis in Swiss albino mice. *Chem Biol Interact*, 242, 345–352. http://dx.doi.org/10.1016/j.cbi.2015.10.020

55 Wang, J., Zhu, H., Yang, Z., & Liu, Z. (2013). Antioxidative effects of hesperetin against lead acetate-induced oxidative stress in rats. *Indian J Pharmacol*, 45(4), 395–398. https://doi.org/10.4103/0253-7613.115015